Applied Mathematical Modelling 39 (2015) 851–861

Contents lists available at ScienceDirect

Applied Mathematical Modelling

journal homepage: www.elsevier.com/locate/apm

Verification of a new CFD compressible segregated and multi-phase solver with different flux updates-equations sequences

Raúl Payri [1], Santiago Ruiz [1], Jaime Gimeno [1], Pedro Martí-Aldaraví *

CMT – Motores Térmicos, Universitat Politècnica de València, Edificio 6D, Camino de Vera s/n, 46022 Valencia, Spain

ARTICLE INFO

Article history:
Received 3 January 2013
Received in revised form 28 May 2014
Accepted 12 July 2014
Available online 22 July 2014

Keywords:
Multi-phase
CFD
OpenFOAM
Verification
Flux update
Fuel injection

ABSTRACT

A new solver capable of calculating liquid and/or gas problems has been developed, verified and validated. Compressible solvers in Computational Fluid Dynamics use both mass flux and volumetric fluxes through the cell surface to calculate derivative terms. These fluxes depend on density and velocity fields, therefore the stability of the solver is affected by "how" and "where" density and velocity are calculated or updated. In addition to verification and validation, this paper deals with how different flux updates-equations sequences change the computational solution, reaching the conclusion that for mono-phase solvers no extra-updates should be used in order to minimize computational cost, but for multi-phase solvers with high density gradients an extra-update should be implemented to improve the stability of the solver.

1. Introduction

Focusing on the automotive area, concretely non-reactive fuel injection studies, it is common to divide the problem into two parts depending on the area of interest and composition of the fluid: internal flow and external flow. Internal flow studies deal with the influence of the injector geometry on the flow pattern [1], the cavitation phenomena [2], the needle lift [3] and eccentricity and other manufacturing issues relevance, etc.; and external flow studies deal with fuel break-up [4,5], atomization and fuel–air mixing processes [6]. This division is made because of the different flow nature: in the internal part the flow is *continuous*, mono-phase liquid (or multi-phase if cavitation is considered); and in the external part far from the injector exit the flow is *dispersed* multi-phase.

If the whole injection process (internal and external flows) is going to be simulated at the same time an Eulerian approach seems to be the best option. A mixture model with a liquid mass fraction that defines the percentage of liquid in the cell is desired rather than a VOF model such the one Srinivasana et al. [7] used. This is due to, far downstream from the nozzle exit, the fuel droplets are very small (5–20 μm in diameter [8]) and then tracking the inter-phase becomes very expensive in computational cost. The main awkwardness of this approach is the break-up model, in other words, how to get a dispersed phase from a continuous one. This issue was solved by Vallet et al. [9], who took the dispersion of droplets into account with a diffusion term and calculated the inter-phase surface with a new balance equation with convection, diffusion, production

* Corresponding author. Tel.: +34 963877650; fax: +34 963877659.
E-mail addresses: rpayri@mot.upv.es (R. Payri), saruiz@mot.upv.es (S. Ruiz), jaigigar@mot.upv.es (J. Gimeno), pedmar15@mot.upv.es (P. Martí-Aldaraví).
[1] Tel.: +34 963877650; fax: +34 963877659.

http://dx.doi.org/10.1016/j.apm.2014.07.011
0307-904X/

Nomenclature

CDV	converging–diverging verification
CFD	computational fluid dynamics
EOS	equation of state
K	kinetic energy of the fluid (m^2/s^2)
PISO	pressure implicit with splitting of operators
Pr	Prandtl number
Pr_t	turbulent Prandtl number
R	gas constant ($m^2/(s^2\ K)$)
Sc	Schmidt number (–)
SIMPLE	semi-implicit method for pressure-linked equations
SOI	start of injection
T	temperature (K)
$\mathbf{U}$	velocity vector (m/s)
VOF	volume-of-fluid
Y_1	liquid mass fraction (–)
Y_2	gas mass fraction (–)
a_P	diagonal matrix of the velocity equation (m/s)
h	enthalpy (m^2/s^2)
p	pressure (Pa)
t	time (s)
Φ	mass flux (kg/s)
Φ_U	volumetric flux (m^3/s)
Ψ	compressibility (s^2/m^2)
κ_{eff}	effective thermal diffusivity (m^2/s)
μ	molecular viscosity (m^2/s)
μ_{eff}	turbulent molecular viscosity, $\mu + \mu_t$ (m^2/s)
μ_t	turbulent molecular viscosity (m^2/s)
ν	kinematic viscosity, $\nu = \mu/\rho$ (m^2/s)
ρ	density (kg/m^3)
τ	Reynolds Stress Tensor (kg/(m s))

and destruction terms. Nevertheless, Vallet et al. model and its further improvements [10–12] calculate the pressure with the EOS or an isentropic relationship between density and pressure, then adding certain hypotheses to the simulation.

A new Eulerian two-phase model has been developed with the aim of simulating internal and external flows at once with a single domain. This new solver uses a pressure equation derived from compressible continuity and momentum conservation equations as described by Jasak [13]. For every new model, verification and validation are the primary means to assess accuracy and reliability in computational simulations [14]. Basically, verification consists of checking the numerics, in other words, checking if the given solution is correct and represents the fundamental physics behind the model; and on the other hand validation consists of checking if the model represents the complexity of real world problems in the scope of study, it means, calculate an error [15]. The main objective of this work is to carry out the *verification* of the new solver by comparing mono-phase solutions (using liquid and gas as working fluids) with analytical solutions for a CDV nozzle problem (as done by Maksic and Mewes [16]) and to fulfill the *validation* by comparing two-phase solutions with experiments. A second objective is to check the performance of the solver with different flux updates along the sequence of equations. Available solvers update the mass (or volumetric) flux through cell faces twice: before (corrected flux) and after (conservative flux) solving the pressure equation. However, correcting or updating fluxes at different positions inside the equations sequence could improve the solver performance.

The main objective of this work is to carry out the *verification* of the new solver by comparing mono-phase solutions (using liquid and gas as working fluids) with analytical solutions for a CDV nozzle problem (as done by Maksic and Mewes [16]) and to fulfill the *validation* by comparing two-phase solutions with experiments. A second objective is to check the performance of the solver with different flux updates along the sequence of equations. Available solvers update the mass (or volumetric) flux through cell faces twice: before (corrected flux) and after (conservative flux) solving the pressure equation. However, correcting or updating fluxes at different positions inside the equations sequence could improve the solver performance.

After validation, the present model can be used to run novel simulation of liquid injections into gaseous atmosphere without making any difference between internal and external flows, then reducing the error during their coupling and allowing, for example, an improvement in the definition of the inlet boundary condition.

2. Methodology

2.1. Code description

The model proposed here is based in the same four principles than the one proposed by Vallet et al. [9]: (1) high Reynolds and Weber numbers, (2) the difference between the mean velocity of the liquid fluid and gaseous fluid particles can be calculated, (3) the dispersion of the liquid phase into the gas phase can be computed by a balance equation, and (4) the mean size of the liquid fragments can be calculated through the mean surface area of the liquid–gas interface per unit of volume.

Instead of the classical PISO algorithm, a PIMPLE approach is used to support partial convergence of intermediate iterations, it can be turned into a PISO or SIMPLE algorithms by selecting the right number of inner and outer loops. PIMPLE algorithm combines the loop structures of PISO and SIMPLE, including $\partial/\partial t$ terms in equations but not limited by Courant number [17]. In every outer loop, the sequence of transport equations is solved as shown in Fig. 1(a), based on Jasak's work [13].

The balance equation for the liquid mass fraction (Eq. (1)), here called Y_1, is the same as in [9]. The break-up and mixing processes, due only to turbulence by hypothesis, are modeled here with a closure term which follows the Fick's law. Nevertheless, any other model could be used [18]. In all equations from now, Φ represents the mass flux, calculated by Eq. (7).

$$\frac{\partial(\rho \cdot Y_1)}{\partial t} + \nabla \bullet (\Phi \cdot Y_1) - \nabla \bullet \left(\frac{\mu_t}{Sc} \cdot \nabla Y_1\right) = 0. \tag{1}$$

Then, the gas mass fraction is calculated as $Y_2 = 1 - Y_1$. The continuity equation can be written classically as:

$$\frac{\partial \rho}{\partial t} + \nabla \bullet \Phi = 0. \tag{2}$$

The mean velocity follows a balance equation (momentum conservation equation) which does not involve any term corresponding to the momentum exchange between phases because it is the mean velocity of both phases [9]:

$$\frac{\partial(\rho \cdot \mathbf{U})}{\partial t} + \nabla \bullet (\Phi \cdot \mathbf{U}) - \nabla \bullet \left(\mu_{eff} \cdot \nabla \mathbf{U}\right) = -\nabla p \tag{3}$$

Note that the Reynolds Stress Tensor term has been already substituted by the turbulent closure terms. The energy equation has been introduced by means of total enthalpy as follows, where $\tau \cdot \nabla \mathbf{U}$ is the viscous dissipation:

$$\frac{\partial(\rho \cdot h)}{\partial t} + \nabla \bullet (\Phi \cdot h) - \nabla \bullet \left(\alpha_{eff} \cdot \nabla h\right) = \frac{\partial p}{\partial t} - \frac{\partial(\rho \cdot K)}{\partial t} - \nabla \bullet (\Phi \cdot K) + \tau \cdot \nabla \mathbf{U}. \tag{4}$$

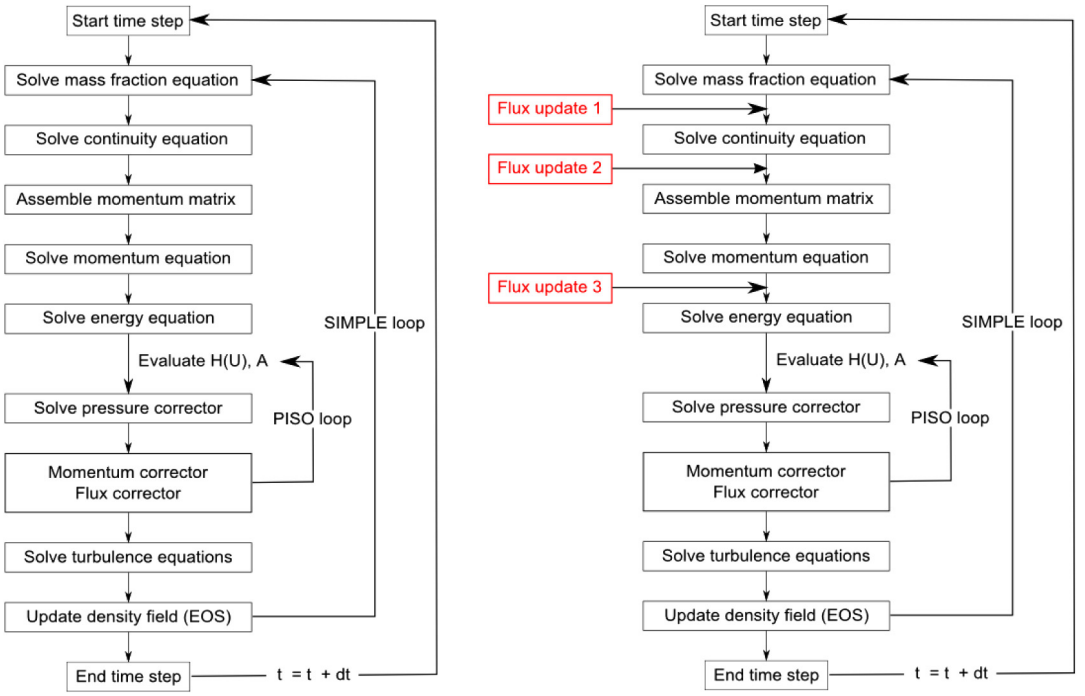

(a) Original sequence. (b) Modified sequence.

Fig. 1. Sequence of equations for the new developed solver.

Finally, the pressure equation derived from continuity and momentum conservation equations in this case is Eq. (5) for transonic simulations and Eq. (6) for low Mach number simulations. The only difference between these two equations is the corrected flux used in the convective term, denoted as Φ_d in the low Mach number case. In both equations the compressibility Ψ of the mixture has been taken as volumetric average of the compressibility of the phases.

$$\frac{\partial(\Psi \cdot p)}{\partial t} + \nabla \bullet (\Phi_d \cdot p) - \nabla \bullet \left(\frac{\rho}{a_P} \cdot \nabla p\right) = 0, \tag{5}$$

$$\frac{\partial(\Psi \cdot p)}{\partial t} + \nabla \bullet (\Phi) - \nabla \bullet \left(\frac{\rho}{a_P} \cdot \nabla p\right) = 0. \tag{6}$$

Inside the PISO loop and also after solving the turbulence equations (see Fig. 1), the density is re-calculated with the EOS presented by Vallet et al. [9]. This ensures that the tight correlation which exists between Y_1 and ρ is accomplished.

Turbulence model and equations to calculate the turbulent viscosity can be selected from the available libraries, or new models more suitable for large density fluctuations such [18,19] could be implemented. RANS (Reynolds-Averaged Navier–Stokes) and LES (Large Eddy Simulation) approaches both are suitable for this new solver. For verification cases, wall slip conditions are considered and no turbulence model is selected. For the validation case, the selected turbulence model is mentioned in the next subsection.

The governing equations just presented are solved using the finite volume CFD code OpenFOAM 2.1.0®, which employs temporal and spatial discretization schemes that are bounded and preserve the proper physical limits on the fluid-dynamics variables. In this study, first order upwind discretization schemes are always used in order to minimize the computational cost, keeping in mind that for validation higher order schemes must be tested.

2.2. Flux updates

The mass flux, a magnitude normal to cell faces (subindex *f*), is calculated as the inner product of the velocity times the density, Eq. (7). The approximation of this equation, although not true in general, is commonly found in compressible solvers because it is acceptable when fields are not strongly non-uniforms (no shocks), such the ones generally found in fuel injection studies, specially inside constant pressure–constant temperature vessels.

$$\Phi = (\rho \cdot \mathbf{U})_f \approx \rho_f \cdot \mathbf{U}_f, \tag{7}$$

$$\Phi = \rho \cdot \Phi_U. \tag{8}$$

It is clear that, if the mesh and cell size are fixed, the flux changes with the density and/or the velocity. Thus, skipping the pressure equation where fluxes are already updated in a conservative way, fluxes can be updated in three different positions along the sequence of equations (see Fig. 1(b)): (1) after mass fraction equation where the density changes because the amount of liquid inside cells changes or, if not, because the density has been updated in the previous time step, (2) after continuity equation, and (3) after velocity equation. In the first two possibilities, Eq. (8) can be used, where Φ_U is calculated inside the PISO loop at the previous time step. But after the velocity equation the volumetric flux has also to be updated and then Eq. (7) is used. Notwithstanding, updating fluxes using the velocity field does not enforce the mass conservation principle because conservation is not enforced on **U** exactly, but on Φ (the flux is the conservative variable, not the velocity). Thus, conservation errors could be introduced by this way.

All possible combinations of three different variables (three updates) with two levels (“yes” if the update is active and “no” if it is not) lead to $2^3 = 8$ cases of interest, as depicted in Table 1. Note that the four first cases include the non-conservative update 3.

Table 1
Test matrix for updated fluxes test.

Case	Update 1[a]	Update 2[b]	Update 3[c]
1	Yes	Yes	Yes
2	No	Yes	Yes
3	Yes	No	Yes
4	No	No	Yes
5	Yes	Yes	No
6	No	Yes	No
7	Yes	No	No
8	No	No	No

[a] Update after mass fraction equation.
[b] Update after continuity equation.
[c] Update after velocity or momentum equation.

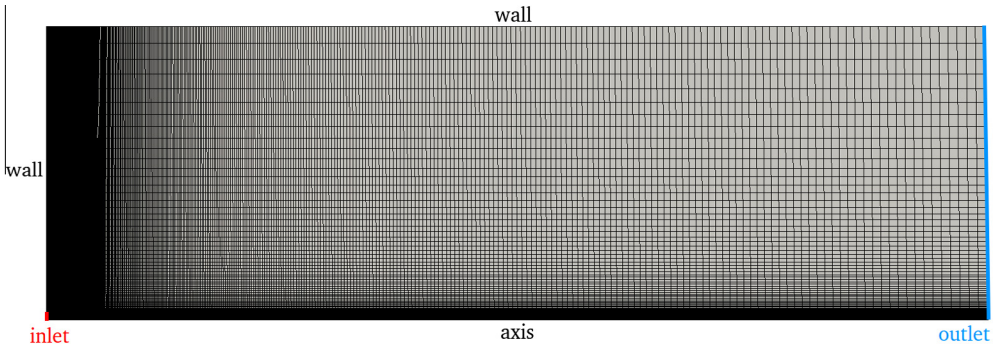

Fig. 2. Axisymmetric domain of 80 × 25 mm (435 × 90 elements) for the validation case.

All of these 8 cases are tested in steady state problems, but the new solver is transient, includes temporal derivative terms. A criterion to determine when the simulation reaches the steady state is needed. In this work, this criterion is that the difference between two following time steps is below 10^{-6} in all variables. The first time step which satisfies this criterion is from now called "convergence time". All verification simulations are carried out with a fixed time step of $5 \cdot 10^{-5}$ s, which gives a maximum Courant number of approximately 1 (0.2 with incompressible fluid).

The computational cost is usually measured with the physical runtime, which however depends on the computer characteristics and load. In order to skip this dependency, the average number of iterations (of U_x variable) per time step is taken instead as value of the computational cost together with the convergence time.

2.3. Validation case

After verification assessment and obtaining the best flux updates-equations sequence, which is to use only update 1 (see next section), validation with a multi-phase problem can be carried out. As a reference case, the work of García-Oliver et al. [20] is exactly reproduced. To summarize, a single-hole diesel injector nozzle is considered, so an axisymmetric domain shown in Fig. 2 can be built.

The orifice outlet radius, inlet boundary length for the domain, is 0.056 mm. The injection pressure is 80 MPa, the ambient density (N^2 gas, with $R = 296.9\ m^2/(s^2\ K)$ and $\nu = 1.46 \cdot 10^{-5}\ m^2/s$) is 40 kg/m^3 and the ambient temperature is 293 K. The injected fluid is standard diesel with $\rho = 822.1\ kg/m^3$, $\nu = 1.12 \cdot 10^{-6}\ m^2/s$ and $\Psi = 4.54 \cdot 10^{-7}\ s^2/m^2$. Non-slip boundary condition is used at walls, constant pressure condition at outlet and time varying velocity condition at the inlet. The velocity value is calculated from experimental mass flow rate measurements [20,21]. The turbulence model selected is high density ratio k–ϵ, developed by Demoulin et al. [18] in purpose for this kind of solvers; and Schmidt and Prandtl numbers were set to 0.9 [20].

3. Results and discussion

3.1. Mesh sensitivity study

Before proceeding with the study, the convergence of the algorithm with regard to reductions in the spatial mesh width needed to be ensured [22]. Mesh resolution was changed from 250 to 10000 elements comparing the Mach number on the axis at the throat position of the CDV nozzle with compressible fluid (case detailed in a posterior section) and without any extra-update. Increasing the number of elements beyond 2500 (100 × 25) does not change the computational solution (differences below 1%). Therefore, this mesh size is chosen for the rest of the studies.

3.2. Incompressible flow problem

The CDV nozzle is shown in Fig. 3. This nozzle is axisymmetric, 1 m in length and has 0.15 m of inlet and outlet radius. The throat is placed 0.25 m from the inlet and has 0.10 m of radius. Boundary conditions are shown in Tables 2–5.

The working fluid is inviscid and incompressible water, which physical properties are well known: $\rho = 1000\ kg/m^3$ and $Pr = 7$. Volumetric flux conservation gives an analytical expression for the velocity depending on the area ratio and inlet velocity, and Bernoulli's principle gives an expression for the pressure. The temperature is assumed to be constant. Thus, errors in velocity, pressure and temperature can be checked.

Table 6 shows the average error and the computational cost (defined as the average number of interactions as explained in Section 2.2) of each case of Table 1. Errors, convergence time (see Section 2.2) and number of iterations per time step are the same regardless the case, meaning that any flux-update affects neither the accuracy nor the computational cost for incompressible problems.

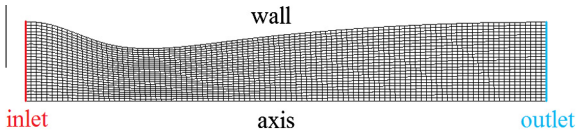

Fig. 3. Converging–diverging verification (CDV) nozzle domain.

Table 2
Y_1 boundary conditions for the incompressible problem.

Patch	Type	Value
Inlet	Fixed value	1
Outlet	Zero gradient	–
Wall	Zero gradient	–
Axis	Empty	–

Table 3
U boundary conditions for the incompressible problem.

Patch	Type	Value
Inlet	Fixed value	10
Outlet	Zero gradient	–
Wall	Slip	–
Axis	Empty	–

Table 4
T boundary conditions for the incompressible problem.

Patch	Type	Value
Inlet	Fixed value	298
Outlet	Zero gradient	–
Wall	Zero gradient	–
Axis	Empty	–

Table 5
p Boundary conditions for the incompressible problem.

Patch	Type	Value
Inlet	Fixed value	10e5
Outlet	Zero gradient	–
Wall	Zero gradient	–
Axis	Empty	–

Table 6
Accuracy and computational cost results for the incompressible problem.

Case	Avg. error [%]	Conv. time [μs]	Avg. $\mathbf{U_x}$ #iters.
1	3.31	230	1.0
2	3.31	230	1.0
3	3.31	230	1.0
4	3.31	230	1.0
5	3.31	230	1.0
6	3.31	230	1.0
7	3.31	230	1.0
8	3.31	230	1.0

Fig. 4 shows the evolution of velocity, pressure and temperature along the axis of the nozzle. The analytical solution is well represented by the 8 cases, the maximum error is placed at the throat (the reason of this difference is explained at the end of the next section). However, a difference of around 2 K between the first four and the other cases can be observed in the temperature distribution (Fig. 4(c)) because the update 3 creates an artificial coupling between velocity and temperature fields.

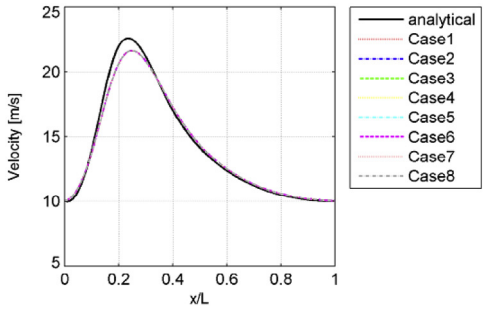

(a) Velocity distribution.

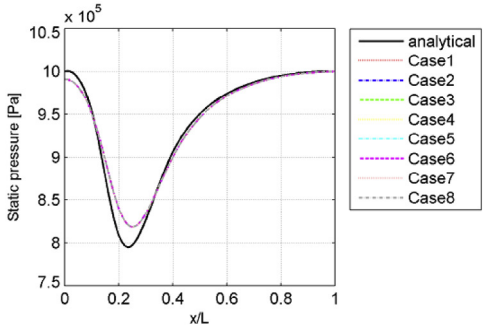

(b) Pressure distribution.

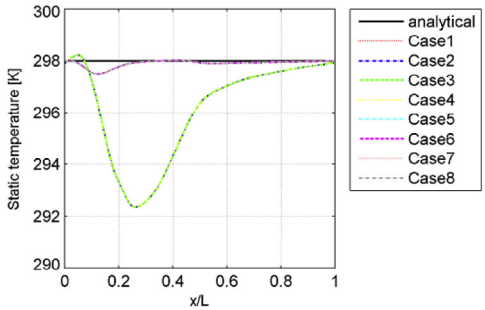

(c) Temperature distribution.

Fig. 4. Incompressible nozzle problem.

3.3. Compressible flow problem

In this case, the working fluid is inviscid air, considered as perfect gas (its physical properties are also well known): $c_p = 1006\ \mathrm{m^2/(s^2\ K)},\ \gamma = 1.4,\ R = 287\ \mathrm{m^2/(s^2\ K)}$. Boundary conditions shown in Tables 1–10 ensure a transition between subsonic flow at the inlet to supersonic flow at the outlet, furthermore the selected pressure drop guarantee that no shock wave is generated in the domain. This problem also has analytical solution, which can be easily found in any compressible fluid dynamics book, for example Ref. [23, Chapter 10]. Thus, errors in Mach number, pressure and temperature can be analyzed.

Table 11 summarizes accuracy and computational cost results, as before. First thing to notice is that updating fluxes with the velocity (non-conservative way) leads to divergence. This means that mass conservation must be ensured along the loop for applications with density gradients. For the other four cases, errors are quite similar regardless the case. Average error is around 6%, so there is a general agreement with the theoretical solution. Nonetheless, update 2 increases the number of iterations per time step probably because the flux used in continuity equation is not the same than in the rest of transport equations, and then more PIMPLE loops are required to reach convergence. Update 1 decreases the convergence time with approximately the same number of iterations per time step, then it reduces computational cost. This happens because the flux is recalculated with the updated density from the previous time step, then reducing differences between time steps.

Fig. 5 shows the evolution of velocity, pressure and temperature along the axis of the nozzle. All 4 cases that converge predict well the analytical solution. Small differences which can be seen in the figures for both, incompressible and compressible problems, are due to "two-dimensional" effects in the simulations. A pressure gradient is obtained in the radial direction of the nozzle, meanwhile the analytical solution assumes that fluid properties and variables are constant in every section, in other words, the flow field depends only on the axial direction.

3.4. Validation problem

Liquid spray penetration, defined as the axial distance where the liquid volume fraction is below 0.1% [20], and the spray angle, defined as the slope of a linear fitting on the spray contour up to the 60% of the spray penetration [1], are the comparison parameters. Experimental values were obtained and published by Payri et al. [21].

Table 7
Y_1 boundary conditions for the compressible problem.

Patch	Type	Value
Inlet	Fixed value	0
Outlet	Zero gradient	–
Wall	Zero gradient	–
Axis	Empty	–

Table 8
U boundary conditions for the compressible problem.

Patch	Type	Value
Inlet	Fixed value	92.52
Outlet	Zero gradient	–
Wall	Slip	–
Axis	Empty	–

Table 9
T boundary conditions for the compressible problem.

Patch	Type	Value
Inlet	Fixed value	298
Outlet	Zero gradient	–
Wall	Zero gradient	–
Axis	Empty	–

Table 10
p Boundary conditions for the compressible problem.

Patch	Type	Value
Inlet	Fixed value	2.075e5
Outlet	Zero gradient	–
Wall	Zero gradient	–
Axis	Empty	–

Table 11
Accuracy and computational cost results of the compressible problem.

Case	Avg. error [%]	Conv. time [μs]	Avg. $\mathbf{U_x}$ #iters.
1	–	–	–
2	–	–	–
3	–	–	–
4	–	–	–
5	6.21	5480	3.6
6	6.14	5500	3.7
7	6.38	5470	3.0
8	6.27	5530	2.8

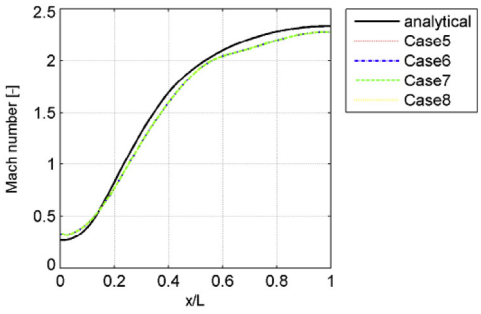

(a) Velocity distribution.

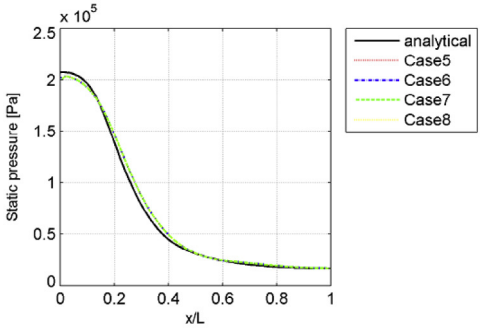

(b) Pressure distribution.

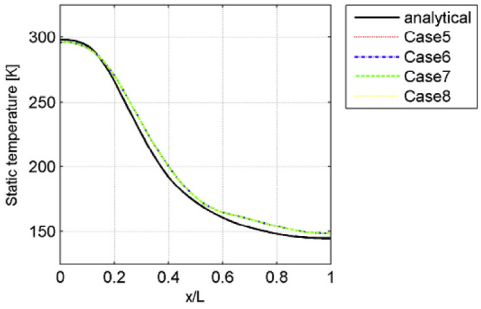

(c) Temperature distribution.

Fig. 5. Compressible nozzle problem.

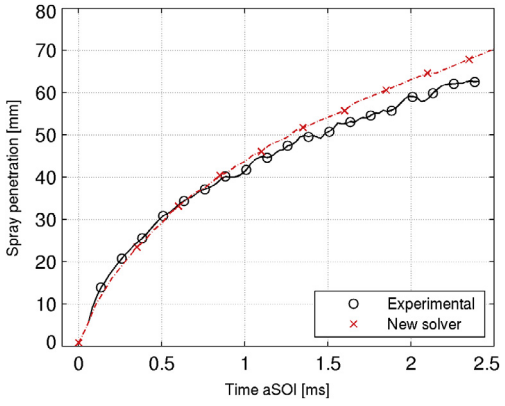

(a) Spray penetration.

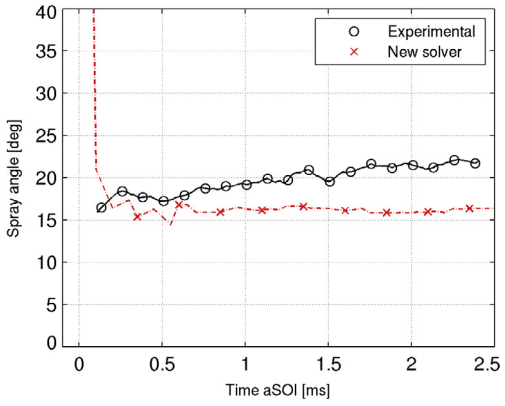

(b) Spray angle.

Fig. 6. Validation single-hole nozzle injector problem.

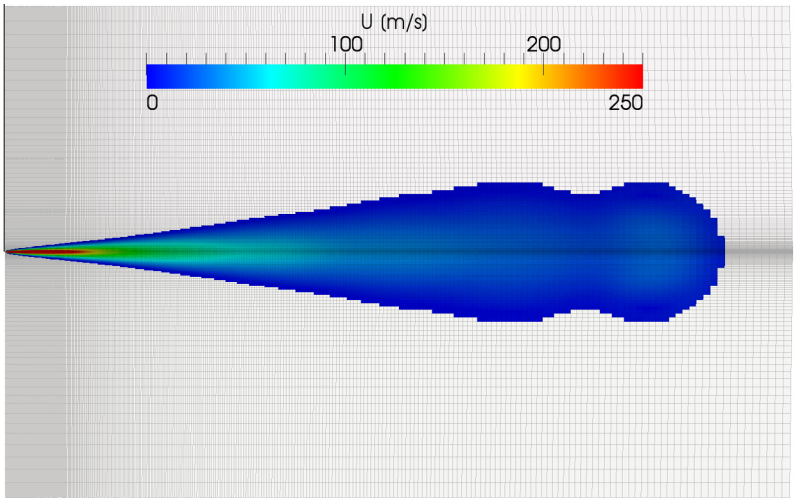

Fig. 7. Contours of **U** inside the spray, $Y \in [0 : 001; 1]$.

Fig. 6(a) shows a very good agreement between experiments and computational results, both curves match until 1.5 ms after SOI. Beyond that point, the error is below 10%. This behavior can be explained analyzing the spray angle on Fig. 6(b). The spray predicted by the new solver is about 5° narrower long time after SOI, so it was expected a shorter penetration [21]. A smaller value for the Schmidt number would result in a wider and shorter spray, but selecting the right values for the model parameters is part of a future work.

Fig. 7 shows velocity contours inside the spray. A threshold has been set to better see the spray structure. The common cone-shaped spray is obtained with the velocity rapidly decreasing on the axis but also in the radial direction. Therefore, the model can be considered validated.

4. Conclusions

A new multi-phase compressible solver has been developed and verified. Obtained solutions with this solver match the analytical ones for incompressible and compressible problems.

Up to 8 updates-equations sequences have been calculated for incompressible and compressible problems. It has been seen that updating fluxes in a non-conservative way leads to divergence when compressible solvers are used, so this option can only be used inside the PISO loop where the internal corrector loop ensures convergence and the flux is calculated at the end in a conservative way from the pressure corrector.

For incompressible solvers, none of the sequences changes the accuracy of the solution neither the computational cost, though the temperature drop is bigger with non-conservative updates. For the compressible problem the accuracy is the same in all cases that converge, but sequences with no updates or only update 1 are slightly faster.

Taking into account that the main objective of this solver is the steady part of the diesel fuel injection, the final proposal for this model is updating the fluxes after the mass fraction equation (update 1, case 7) because of its slightly lower computational cost. This way, for multi-phase simulations mass fraction and density fields are consistent in every iteration of every time-step.

With this configuration of the solver,the validation assessment was carried out. A single-hole nozzle injector which is experimentally well characterized has been simulated. Results match experimental penetration values until 1.5 mm after SOI and the spray structure is the one experimentally observed, so the solver and the flux updates-equations sequences have been validated. There is still work to do to correct the behavior of the spray long time after SOI.

Acknowledgments

This research was funded in the frame the project "Comprensión de la influencia de combustibles no convencionales en el proceso de inyección y combustión tipo Diésel" reference TRA2013-36932 from Ministerio de Enonomía y Competitividad (Spanish Ministry of Economy).

References

[1] J.M. Desantes, R. Payri, J.M. Pastor, J. Gimeno, Experimental characterization of internal nozzle flow and diesel spray behavior. Part 1: Non-evaporative conditions, Atomization Sprays 15 (2005) 489–516.

[2] F. Payri, R. Payri, F.J. Salvador, J. Martínez-López, A contribution to the understanding of cavitation effects in Diesel injector nozzles through a combined experimental and computational investigation, Comput. Fluids 58 (2012) 88–101.
[3] Y. Wang, W.G. Lee, R.D. Reitz, Numerical simulation of diesel sprays using an Eulerian–Lagrangian spray and atomization (ELSA) model coupled with nozzle flow, SAE International 2011-01-0386, 2013.
[4] R. Payri, F.J. Salvador, J. Gimeno, R. Novella, Flow regime effects on non-cavitating injection nozzle over spray behaviour, Int. J. Heat Fluid Flow 32 (2011) 273–284.
[5] J.M. Desantes, R. Payri, F.J. Salvador, J. De la Morena, Influence of cavitation phenomenon on primary break-up and spray behavior at stationary conditions, Fuel 89 (2010) 3033–3041.
[6] R. Payri, J. Gimeno, P. Martí-Aldaraví, J. Manin, Fuel concentration in isothermal Diesel sprays through structured planar laser imaging measurements, Int. J. Heat Fluid Flow 34 (2012) 98–106.
[7] V. Srinivasana, Abraham J. Salazarb, Kozo Saitoc, Modeling the disintegration of modulated liquid jets using volume-of-fluid (VOF) methodology, Appl. Math. Modell. 35 (2011) 3710–3730.
[8] J.V. Pastor, R. Payri, J.M. Salavert, J. Manin, Evaluation of natural and tracer fluorescent emission methods for droplet size measurements in a diesel spray, Int. J. Automot. Technol. 13 (2012) 713–724.
[9] A. Vallet, A.A. Burluka, R. Borghi, Development of a Eulerian model for the atomization of a liquid jet, Atomization Sprays 11 (2001) 619–642.
[10] W. Ning, R.D. Reitz, Development of a next-generation spray and atomization model using an Eulerian–Lagrangian methodology, in: 17th International Multidimensional Engine Modeling User's Group Meeting, Detroit MI, USA, 2007.
[11] S. Hoyas, A. Gil, X. Margot, D. Khuong-Anh, F. Ravet, Evaluation of the Eulerian–Lagrangian spray atomization (ELSA) model in spray simulations: 2D cases, Math. Comput. Modell. 57 (2013) 1686–1693.
[12] N. Trask, D.P. Schmidt, M.D.A. Lightfoot, S.A. Danczyk, Compressible modeling of the internal flow in a gas-centered swirl-coaxial fuel injector, J. Propul. Power 28 (2012) 685–693.
[13] Hrvoje Jasak, Error analysis and estimation for the finite volume method with applications to fluid flows, Department of Mechanical Engineering, Imperial College of Science, Technology and Medicine, June, 1996.
[14] W.L. Oberkampf, T.G. Truncano, Verification and validation in computational fluid dynamics, Prog. Aerosp. Sci. 38 (2002) 209–272.
[15] A.I.A.A. Staff, AIAA Guide for the Verification and Validation of Computational Fluid Dynamics Simulations, American Institute of Aeronautics & Astronautics, USA, 1998.
[16] S. Maksic, D. Mewers, CFD-calculation of the flashing flow in pipes and nozzles, Am. Soc. Mech. Eng. Fluids Eng. Div. 257 (2002) 511–516.
[17] Silicon Graphics International Corp., OpenFOAM. User Guide. Available on-line (accessed on January, 2012), <http://www.opencfd.co.uk>.
[18] F.-X. Demoulin, P.-A. Beau, G. Blokkeel, A. Mura, R. Borghi, A new model for turbulent flows with large density fluctuations: application to liquid atomization, Atomization Sprays 17 (2007) 315–345.
[19] T.H. Shih, W.W. Liou, A. Shabbir, Z. Tang, J. Zhu, A new k–epsilon eddy viscosity model for high Reynolds number turbulent flows, Comput. Fluids 24 (1995) 227–238.
[20] J.M. García-Oliver, J.M. Pastor, A. Pandal, N. Trask, E. Baldwin, D.P. Schmidt, Diesel spray CFD simulation based on $\Sigma - Y$ Eulerian atomization model, Atomization Sprays 23 (2013) 71–95.
[21] R. Payri, F.J. Salvador, J. Gimeno, R. Novella, Flow regime effects on non-cavitating injection nozzles over spray behavior, Int. J. Heat Fluid Flow 32 (2011) 273–284.
[22] Y. Wang, H.-W. Ge, R.D. Reitz, Validation of mesh- and timestep- independent spray models for multi-dimensional engine CFD simulation, SAE Int. J. Fuels Lubr. 3 (2010) 277–302.
[23] J.D. Anderson Jr., Fundamentals of Aerodynamics, McGraw-Hill, Singapore, 2007.